In-fibre fabry-perot cavity sensor for high temperature applications

In-Fibre Fabry-Perot Cavity Sensor for High Temperature Applications

Jinesh Mathew, Oliver Schneller, Dimitrios Polyzos, Dirk Havermann, Richard M. Carter, William N. MacPherson, Duncan P. Hand and Robert R.J. Maier

***Abstract*—The fabrication, characterization and encapsulation of a fibre optic temperature sensor based upon a micro Fabry-Perot (F-P) cavity is presented. The F-P cavity is formed between a reflective in-fibre metallic splice and the air-fibre boundary at the end of the sensor. A change in temperature modifies the optical cavity length and this is observed as a change in the reflected interference spectrum. The sensor has been demonstrated for high temperature measurement up to 1100 °C. The stability of the sensor system is ~10 °C over a period exceeding 300 hours at 1100 °C. Furthermore a sealed capillary is used as a protective enclosure.**

***Index Terms*—Fabry-Perot cavity, optical fiber sensors, optical fiber devices, temperature sensors, metal thin-film, strain isolation.**

I. INTRODUCTION

Temperature is one of the most widely measured parameters within industry and science. In many applications sensors are required which are immune to electromagnetic interference, are small and light weight, allow operation in hazardous environments, have high sensitivity and wide operating range and allow interrogation over long distances without electronic / electrical interface. Fibre optic sensors offer an excellent solution to many of these challenges. Different fibre optic sensor techniques have been demonstrated for temperature measurements up to ~1100 °C when based on fused silica fibres or, at even higher temperatures (>1500 °C), with Sapphire fibres. Fused silica based high temperature sensors with useful spatial resolutions (<50 mm) include fibre Bragg grating (FBG) sensors [1-6] and Fabry-Perot (F-P) fibre-optic sensors [7-9]. Sapphire crystal temperature sensors have been demonstrated based on; a thermally emissive source embedded inside one end of a sapphire rod [10,11], fibre Bragg gratings inside a sapphire rod [12,13], or based on a F-P cavity [14-16]. Sapphire crystal based temperature sensors have the potential for monitoring temperatures in excess of 1500 °C but here the fibre is a multimodal rod (outer diameter >50 µm) of sapphire without a cladding. Interrogation of sapphire fibre sensors is difficult when compared to a FBG or F-P sensor using standard single mode optical fibre systems. Although recently developed FBGs such as; regenerated gratings [1-4], chemical-composition gratings [5], and surface relief gratings [6] have been shown to be capable of temperature measurements at temperatures in excess of 1000 °C, the long term stability of these FBGs at high temperature has not yet been proven sufficiently to allow their use in applications which require high stability over extended periods of time while operating at temperatures of up to 1100 °C.

In the case of a F-P cavity, the sensor is formed by a well defined interface between two materials where the optical path length is depended on the temperature of the material in the cavity. In this paper we focus on F-P type sensors as a potential solution for reliable high temperature fibre optic sensing. The results presented in this paper are an extended version of the preliminary results presented by the authors at the OFS-23 conference [9]. Other F-P sensors previously reported for high temperature monitoring and compatible for a standard single mode fibre based interrogation are made by incorporating dielectric mirrors into a continuous length of a single mode fibre [7], or by splicing a short section of all-silica photonic crystal fibre at one end of a single mode fibre [8]. The internal mirror for the former sensor is obtained by introducing a 100 nm layer of TiO_2 between the fibre splices. Two such reflective splices are incorporated with a separation of 1.5 mm. This sensor has been demonstrated for operation up to 1050 °C. The sensors in [8] have dimensions of 575 µm and 4.78 mm and have been demonstrated for sensing up to 1200 °C for two short duration thermal cycles. This sensor is affected by multimodal interference due to the mismatch in the core of the fibres; which makes the interrogation of the sensor more complex and thus difficult. The important information missing for all the above mentioned fibre optic high temperature sensors are their stability at high temperatures. A sensor should be stable at its operational temperature over a long period of time to achieve a reliable continuous measurement. This paper presents detailed results on the long term stability of a fibre optic temperature sensor at high temperatures.

The F-P cavities presented in this paper has dimensions ≤125 µm, suitable for a point measurement and has a spatial resolution smaller than the sensors in [7,8]. In this work chromium (Cr), which has a melting point of 1907 °C is used for making the reflective splice. This melting temperature is slightly higher than that of TiO_2 (1843 °C) used in [7], which enhances the survival of the coating during a fibre fusion

Manuscript received September 05, 2014; revised December 12, 2014; accepted January 20, 2015. Date of publication xxx xx, xxxx; date of current version January 28, 2015. This work was supported in part by the EPSRC and the EU project under Grant 310279.

The authors are with the Applied Optics and Photonics Group, Institute of Photonics and Quantum Sciences, SUPA, Heriot-Watt University, Edinburgh, EH14 4AS, UK e-mail: Jinesh.Mathew@hw.ac.uk.

splicing process and is expected to provide more stability at high temperatures. This is the first time a detailed study of high temperature long term stability of a fibre optic sensor is reported. This strain isolated fibre optic sensor demonstrated for high temperature (>1000 °C) operation is novel.

The F-P cavity is formed between an in-fibre Cr layer and the fibre-air boundary at the end of the sensor as illustrated in Fig. 1. Two different sensor geometries are presented. One is based on conventional single mode fibre (125 µm diameter, Fig. 2) throughout and a second geometry where the sensor cavity is fabricated from reduced diameter fibres (80 and 50 µm, Fig. 3). Repeated long term thermal characterisation studies of these sensor structures show that they are suitable for high temperature measurement up to 1100 °C. Both the sensor types are then encapsulated in a suitable glass capillary to allow for easy incorporation into engineering structures and for strain independent temperature monitoring.

II. EXPERIMENTAL INVESTIGATION AND DISCUSSIONS

The sensor concept is shown schematically in Fig. 1 which portrays a thin reflective metal film sandwiched between two single-mode fibres.

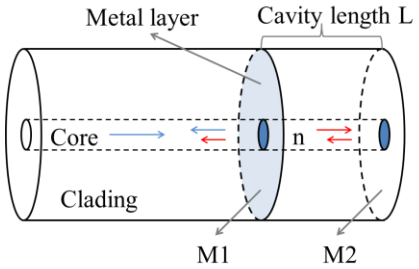

Figure 1. Basic structure of the optical fibre sensor

The first type of sensor is made from conventional single mode fibre throughout. Sensor fabrication starts by preparing the fibre end. The acrylate coating is removed by dipping it in paint stripper (Nitromors ™) for 10-20 minutes and by a subsequent wiping using a lens cleaning tissue and IPA. Immediately following fibre cleaving, a thin layer of Cr is deposited on the fibre tip using an RF sputter coating system. The reflectivity of the applied Cr coating to the fibre tip is monitored during the process using a broad band light source and a 2x2 coupler, where the reflectance is determined by comparison with the ~3.6% Fresnel reflection from an uncoated fibre end (mode effective refractive index of 1.468 at 1550 nm). The coating process is stopped when the reflectivity is approximately 10%. The above reflectivity is valid for a glass/metal/air system, however when spliced up with a continuing fibre, creating a glass/metal/glass system, the reflectivity drops to ~4%. The theoretical thickness to get an (ideal) 4% reflection obtained using the thin film design software, MacLeod is ~4 nm. The splicing is carried out using a filament fusion splicing system (FFS 2000, Vytran Corporation). A reflectivity of around 3.6% at the glass to metal transition, matches the reflectivity of the fibre-air interface and results in a fringe visibility approaching 1. Splice parameters are also optimised to achieve the maximum breaking strength while maintaining the optical properties of the Cr interface between the fibres. A breaking strength of 3.2-5 N is achieved for the reflective splice while the breaking strength of a conventional single mode fibre splice using the same splicing system is 11-15 N. Small (~µm) misalignment during the splicing process causes significant losses in reflectivity and also results in mechanically weak splices that tend to break during subsequent handling. In order to achieve a desired length of cavity the fibre containing a reflective splice was positioned in a fibre cleaving tool (FK11, PK Technology Ltd). It was possible to identify the position of the splice by inspection using a microscope and, with the help of a calibrated scale, the fibre was positioned to allow a cleave at a measured distance (accuracy ±10 µm) from the splice. Thus a F-P cavity is formed between the reflective splice and the low-reflectivity interface between the cleaved end of the fibre and the surrounding atmosphere. Cavity lengths of 20-200 µm were produced using this technique, and a typical image of a sensor is shown in Fig. 2.

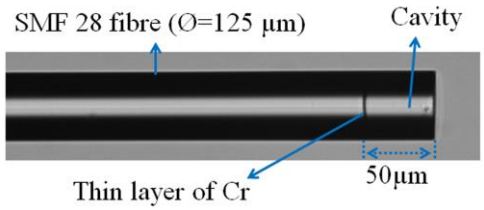

Figure 2. Image of the fabricated 125 µm diameter sensor

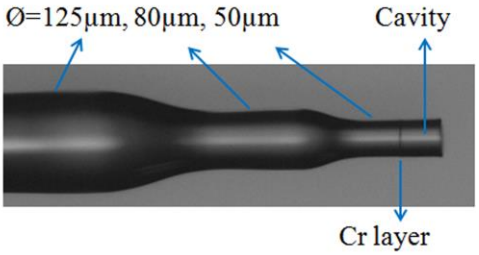

Figure 3. Image of the fabricated 50 µm sensor

The reflection spectrum of the in-fibre F-P cavity depends upon the optical length of the cavity. A change in cavity length produces a change in the periodicity of the interferogram (the free spectral range) and also a shift in the fringe position (phase shift), and thus, a change in the intensity of reflected (or transmitted) optical power at any given wavelength (λ). For a low finesse F-P cavity, the value of round-trip propagation phase φ and value of the optical phase shift $\Delta\varphi$ as a function of temperature[17] are given by

$$\varphi = \frac{4\pi n L}{\lambda} \quad ; \quad \Delta\varphi = \frac{4\pi n L}{\lambda}\left[\frac{1}{n}\frac{dn}{dT} + \frac{1}{L}\frac{dL}{dT}\right]\Delta T \qquad (1),(2)$$

where: n is the effective refractive index of the core mode of the fibre forming the cavity, L is the length of the cavity and dn/dT, dL/dT are the thermo-optic coefficient (~8.6×10^{-6}K^{-1} at ~20 °C) and thermal-expansion coefficient (~0.55×10^{-6}K^{-1}) of the silica fibre respectively [18].

In order to test the sensor for measurement of temperature we inserted the fabricated sensor and a reference thermocouple into separate silica capillaries and placed them into a tube furnace (5415, Lenton thermal designs Ltd). The spectra were recorded using a swept wavelength interrogator (sm125-500, Micron Optics) where the source is a high power, low noise swept wavelength laser, realized with fibre Fabry-Perot tunable filter technology. The recorded data (reflected light intensity values over a wavelength range of 1510-1590 nm, 16K data points) were collected and processed using LabVIEW software. A typical cavity reflection spectrum of a 125 µm diameter sensor is shown in Fig. 4. The interferogram (also called channelled spectrum in the case of an F-P cavity) shown in Fig. 4 has a fringe visibility of ~0.75 and this is well suited to the requirements of the analytical routine used for these sensors. Fringe visibilities close to 1 have also been obtained. The data reduction and extraction of the sensor temperature involves multiple stages of data manipulation, including conversion from an equal stepped spectrum in the wavelength domain to an interpolated, equal stepped spectrum in the optical frequency domain, applying a FFT analysis to determine the fundamental frequency of the optical periodicity, non-linear least square fitting of a sinusoidal function to the spectral data (the frequency of the optical periodicity from the FFT is the initial fitting parameter) and determination of the phase and frequency of the sinusoid [19,20]. The fundamental frequency of the spectra and the phase shift of the sinusoidal fitting were extracted from this data while the furnace temperatures varied and an independent measurement of temperature from the thermocouple was recorded at the same time.

Due to the high sensitivity, wide temperature range and variable starting phase of the sensors, phase ambiguity is observed. This means that some phase values might represent two or more different temperature values. The optical periodicity of the sensor signal is, however, unique for all temperature values and can be used to eliminate the 2π phase uncertainty, hence a combination function of phase and periodicity is used for an unambiguous temperature determination.

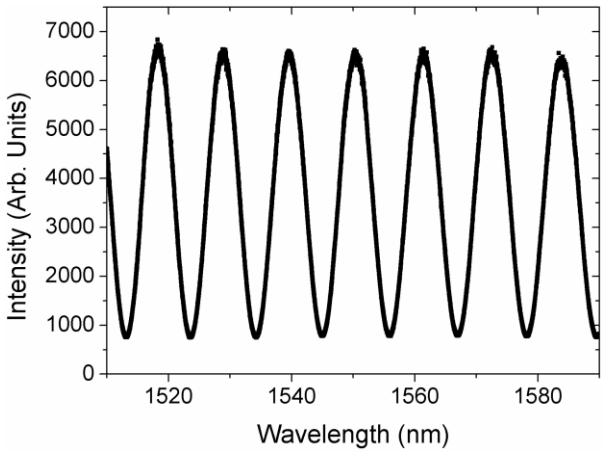

Figure 4. Spectra recorded from the F-P cavity

It is worth noting that the absolute phase of the sensor transfer function depends on the mirror reflectivity, internal reflector losses and is especially sensitive to the exact cavity length [21, 22]. Due to manufacturing tolerances we are unable to generate a cavity length of sufficient accuracy to achieve a specific phase response at a reference temperature. In order to achieve this for an absolute temperature accuracy of ~1°C the length of a typically 70 µm long cavity would need to be known to an accuracy of ~0.5 nm which would be highly challenging. Hence, each sensor has to be calibrated with respect to the phase of the approximated sinusoidal transfer function at a reference temperature. The small, but non zero absorption losses in the intermediate Cr reflection layer introduce a distortion to the sinusoidal transfer function which introduces a systematic offset in the recovered phase measurement. However this distortion is very small for a low finesse cavity and is constant over the whole range of operating conditions. This offset is already contained in the phase measurement at the reference temperature, thus it is calibrated out of the measurement.

Initial temperature cycling was carried out between 25 °C to 600 °C, and then the maximum furnace temperature was increased in steps of 100 °C from 600 °C to 1000 °C. It can be seen from Fig. 5 that in a temperature range of 25 °C–1000 °C, the phase shift has a slightly non-linear relationship with temperature. This is due to the nonlinearity of the thermo-optic coefficient of SiO_2, [23] and has been reported for FBGs in [24]. Taking this into account, the temperature response of the sensor closely follows the theory. The sensitivity of the sensor (cavity length ~55 µm) is in the order of 0.2 degrees/K @100°C, rising to 0.4 degree/K @1000°C. The temperature resolution of the sensor was calculated by analysing the slope and the peak to peak noise level in the calibration curve and it was found to be <10 °C, for a 1s measurement time and <4 °C for a 10 measurement average. During the initial few heating cycles of the sensor a small drift was observed, indicating annealing processes taking place which are attributed to a relieving of stresses in the fusion splice region of the sensor.

We are aiming for sensor components that are on a similar (sub mm) scale to that of the fibre, to allow for easy incorporation into engineering structures.

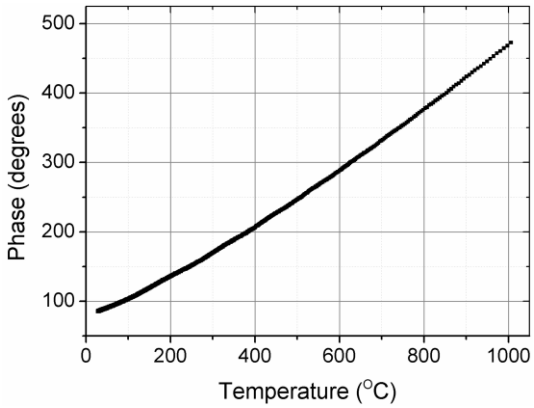

Figure 5. Temperature response of a sensor with cavity length 55 µm between ambient and 1000 °C

For example, to make steam engine or jet engine components smart/intelligent, a small material discontinuity such as a fibre optic sensor can be incorporated in it without degrading structural integrity of the component. Therefore with the requirement to maintain the outer diameter of the sensors as small as possible a second miniaturised sensor structure was developed (Fig. 3). A segment of 80 µm fibre was spliced onto standard SMF28 fibre and then a further segment of a 50 µm is attached to this. A similar thin layer of Cr as given above is applied to the cleaved end of the 50 µm fibre and it is then spliced to another 50 µm fibre. The 50 µm fibre is then cleaved at a measured distance from the splice to form a Fabry-Perot cavity. In order to test the ability and performance of this sensor structure for temperature measurements, we used the same temperature test setup described earlier. As before, the phase shifts non-linearly with increasing temperature. The sensitivity of the sensor (cavity length ~59 µm) is in the order of 0.28 degrees/K @ 100°C, rising to 0.48 degrees/K @ 1000°C. The increase in sensitivity is due to slightly larger cavity length of this F-P sensor. A comparison of the temperature response of F-P sensors with different cavity lengths is shown in Fig. 6. The graph shows the total phase shift of the sensors from 22 °C to 900 °C. A longer cavity has shorter fringe spacing therefore the refractive index change of the fibre required to make a 2π phase shift is smaller than that for a short cavity. As a result the phase shift corresponding to a temperature change increases with an increase in cavity length indicating a higher sensitivity for longer cavity lengths. It is worth noting that the resolution of the interrogator is a constant therefore the signal to noise ratio decreases with cavity length.

In order to evaluate the long term stability, the temperature responses of the sensors have been monitored continuously for over four months at high temperatures between 700 °C to 1150 °C with a step increments of 50 °C. Some results of this study are given in Fig. 7 for the first increase and decrease (cycle 1). We have observed a significant drift of the sensor response above 1100 °C. After this annealing at or above 1150 °C the sensor response shows good long term stability at high temperatures up to 50-100 °C below the annealing temperature. It is observed that the sensor response improved its stability at high temperatures after a second cycling similar to the above. Fig. 8 shows the stability improvement of the

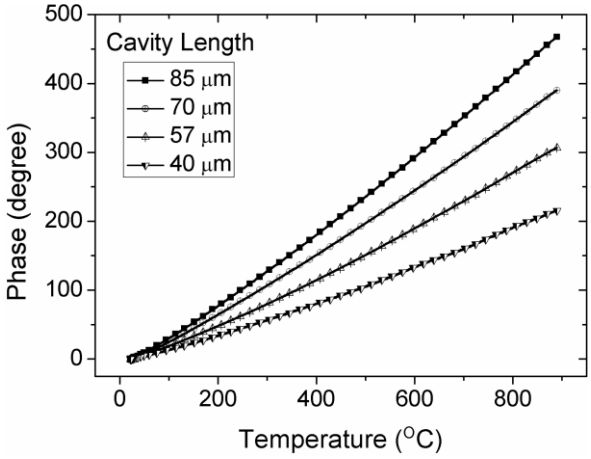

Figure 6. Temperature response of F-P sensors with different cavity length shows variation of its sensitivity.

sensor at 1000 °C during these two cycles where (a) Dark (broader) curve represents the sensor response at 1000 °C over time during the temperature increase step of 1st cycle, similarly (b) represents 1st cycle decrease, (c) represents 2nd cycle increase and (d) represents 2nd cycle decrease. The inside (red/narrow) region in Fig. 8 represents the noise level of the sensor after a ten point averaging where the noise is reduced to one third of the original noise. The peak to peak noise level of the sensor at 1000 °C in Fig. 8(d) is <2 °C after

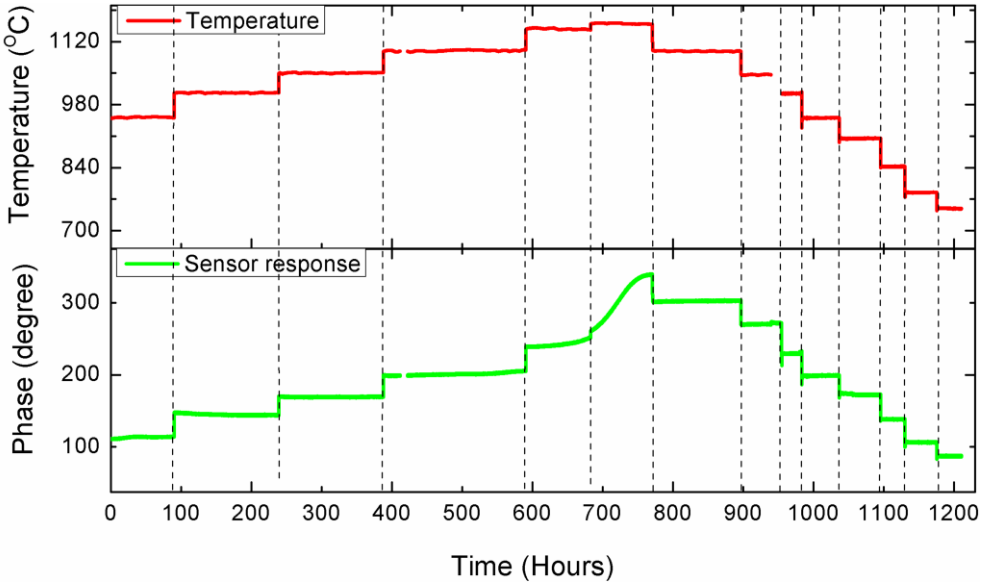

Figure 7. Long term stability of the sensor at high temperatures, upper curve represents the temperature values the sensor is exposed and the lower curve represents the phase values of the sensor signal at these temperatures. Sensor response shows a phase drift at ≥1150 °C over time. After this annealing at or above 1150 °C the sensor response shows good long term stability 50-100 °C below the annealing temperature.

the 10 point averaging and over two days of its operation. The noise level of the sensor at 1100 °C is shown in Fig. 9 which is also <2 °C after the 10 point averaging. The drift of the sensor at 1100 °C is <10 °C for a period of ~300 hrs (Fig. 7) indicating a long term stability of ~10 °C over this period. The results shows that the sensor can be used for reliable temperature measurements up to 1100 °C with an accuracy better than 10 °C.

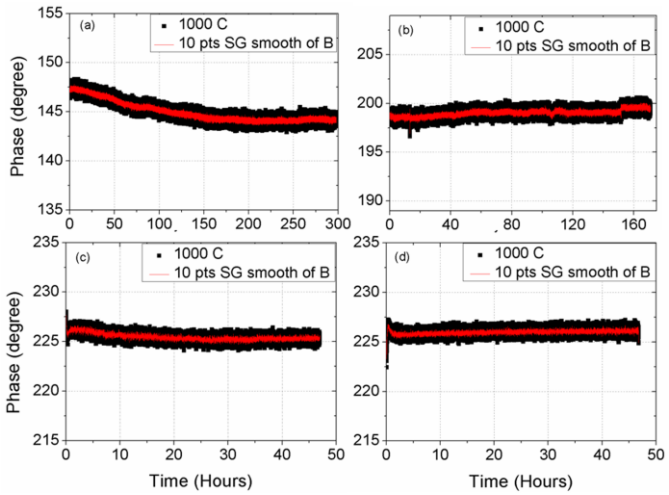

Figure 8. Stability of the sensor at 1000 °C during different stages of the stability analysis routine followed, (a) 1st cycle increase, (b) 1st cycle decrease, (c) 2nd cycle increase and (d) 2nd cycle decrease. Inside (red/narrow) region represents the stability after a 10 point averaging.

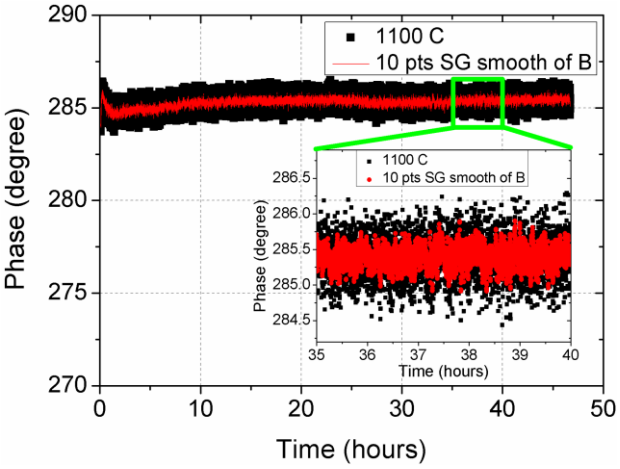

Figure 9. Peak to peak noise of the sensor at 1100 °C, broader curve is before averaging and inside (red/narrow) region is after 10 point averaging.

In order to incorporate our sensor into engineering structures, and to avoid any strain transfer from the surrounds during temperature measurement, suitable strain-relief packaging is required.

Initially electric arc based silica capillary encapsulation is tried for the sensors with outer diameter 125 µm. The used capillary (Z-FSS-150240, Postnova) has a wall thickness of ~35 µm. The energy of the arc required to melt the capillary sufficiently to seal the capillary-fibre interface caused substantial transmission loss thereby, degrading the sensor signal to the detriment of overall signal recovery. Therefore, we have used high temperature compatible glue (water glass) for sealing the capillary-fibre interface. The capillary used has an ID of 150 µm and OD of 220 µm. Initially the polyimide jacket of the capillary was removed using low power arcs of a fusion splicer. The sensor fibre was inserted into the capillary using the micro translation block and associated camera set up of the fusion splicer. Then a small amount of glue was applied to a length of 100-200 µm of the capillary fibre interface. The fibre was rotated to uniformly spread the glue throughout its circumference. The sensor was heated above 100 °C for an hour and kept at room temperature for a day to evaporate the solvent and to set the glue. The glue was also tested for its strength after operating at 1100 °C for 24 hrs. The measured breaking force is ~20 $N.mm^{-2}$. After sealing the capillary-fibre interface, the whole sample was moved and the capillary was sealed off a few hundred micrometers away from the sensor tip using an electric arc. The encapsulated 125 µm sensor is shown in Fig. 10.

In the case of the 50 µm sensor the reduction in the outer fibre diameter allows fusion splicing of a silica capillary (TSP100170, CM Scientific) with 100 µm inner and 150 µm outer diameter onto the 80 µm sensor fibre. Furthermore, the 50 µm diameter sensor tip is suspended inside the capillary without touching the sides, thereby ensuring no strain transfer to the sensor cavity. The capillary was secured to the 80 µm fibre using a fusion splicer (BFS 50, 'BIT' Instruments). By using the attached microscope of the splicer the sensor was inserted into the capillary and aligned. To encourage the collapsing of the capillary a membrane vacuum pump was connected to the end of the capillary. An arc power corresponding to a ~15 mA current is applied to the fibre capillary interface for ~0.5 sec to seal it. After splicing the capillary to the 80 µm fibre, the whole sample was moved ~400 µm and the capillary was sealed off using a further arc heating process (~19 mA, ~0.7 sec). The encapsulated 50 µm sensor is shown in Fig. 11. The surface tension and adhesion to the internal fibre cause a reduction in capillary's outer diameter to ~125 µm in the region where it is melted and fused on to a smaller diameter (80 µm) fibre (Fig. 11).

In order to test the performance of a capillary encapsulated sensor under external strain influences, a metallic jacket was applied to it. The principle is that the Coefficient of thermal expansion (CTE) of the jacket and fibre material silica are different so a temperature change will exert an external strain on the capillary encapsulated sensor.

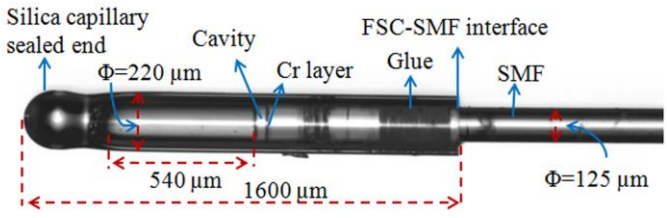

Figure 10. Silica capillary encapsulated 125 µm F-P sensor

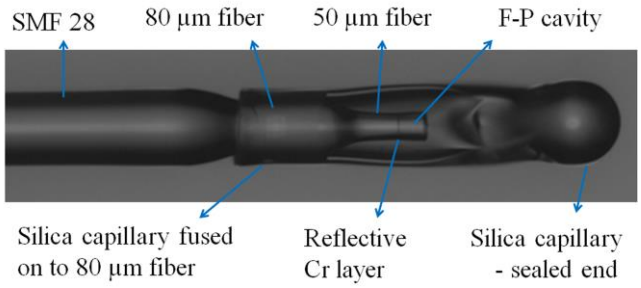

Figure 11. Silica capillary encapsulated 50 µm F-P sensor

Initially silver (Ag) layers are applied to outside of the encapsulated sensor (~80 mm length) using the electro less deposition process [25]. A solution containing the silver nitrate (Tollen's reagent) and a reducing sugar (glucose) react to form Ag, which is deposited on the capillary/fibre. The Ag layer provides the anode for a subsequent nickel (Ni) electroplating process. A Ni layer is applied to the Ag coated fibre by an electro plating process in a Ni-sulphamate bath [26]. The spectrum of the sensor before encapsulation and after encapsulation and metalizing are the same implying no transmission loss introduced during the encapsulation process. A high frequency component appeared in the spectra when the sensor tip is sitting very close (<1 mm) to the sealed end of the capillary because of the reflections from it. This is avoided by maintaining a longer distance (>1 mm) between them.

The metalized F-P sensor was placed in an oven and its thermal response is studied. It was observed that the sensor fibre breaks at temperatures above 200 °C. We speculate that the metallic jacket (~80 mm) present in the region of sensor fibre having no capillary encapsulation is straining the fibre due to their CTE mismatch. Therefore we have redesigned our encapsulation such that capillary sits outside the metallised region.

A capillary (Z-FSS-150240, Postnova) of length ~300 mm was taken, one end sealed using an electric arc. Then 60 mm of the polyimide jacket was removed from the sealed end by dipping it in hot (200 °C) sulphuric acid. An 80 mm long metallic jacket is applied on the capillary, the thickness of the Ag and Ni layers of the jacket are ~5 µm and 160 µm respectively. The other end of the capillary is cleaved using a fibre cleaving tool (FK11, PK Technology Ltd). A 125 µm diameter F-P sensor with a cavity length ~74.5 µm and with a fibre jacket removed length of 295 mm is inserted into the capillary. The capillary-fibre interface is sealed using a 40 mm long fibre sleeve. A schematic diagram of the F-P sensor inside metallised capillary is shown in Fig. 12. This configuration of the sensor is very robust and handy for test under extreme environments. The thermal response of the metallised sensor was studied as explained above. The measured temperature sensitivity of the sensor @ 400 °C is 0.47 degrees/K (Fig. 13) which is same as the sensitivity of an F-P sensor without any encapsulation at 400 °C. This indicates that the encapsulated sensor is well isolated from any external strain influences.

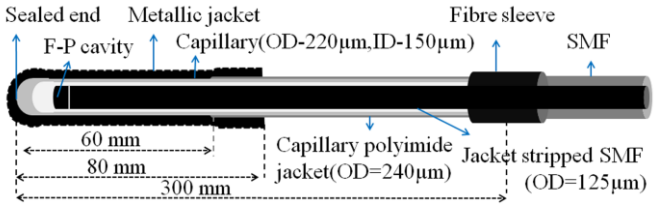

Figure 12. F-P sensor inside metallised capillary, an arrangement for testing external strain influences.

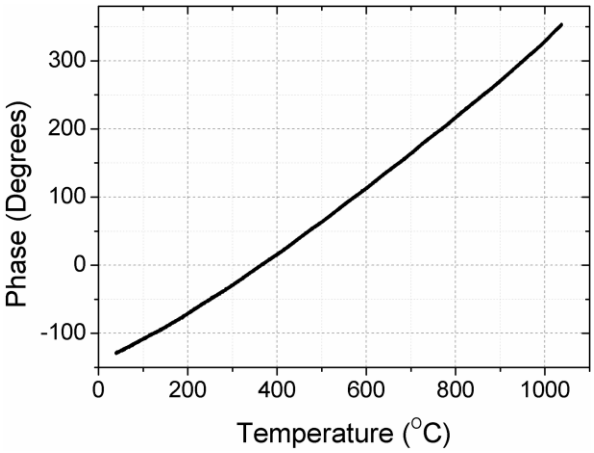

Figure 13. Temperature response of a capillary encapsulated sensor with cavity length 74.5 µm inside a metallic jacket.

III. Conclusion

In conclusion, simple sensor based on an in-fibre F-P cavity for the measurement of high temperature is described. The sensor head consist of an optical fibre end and a reflective splice to form the optical cavity. The relationship between the temperature and the phase is analysed. It has been shown that the temperature information can be calculated from the measurement of the phase shift. A combination of phase and periodicity of the sensor signal is used for an unambiguous determination of the temperature. The key advantage of the sensor demonstrated in this paper is that it can reliably be used for monitoring temperatures up to 1100 °C after annealing. The temperature resolution of the sensor is found to be smaller than 4 °C and the long term (300 hrs.) stability of the sensor is ~10 °C. Silica capillary encapsulation isolates the sensor from any external influences and would, for example, permit the sensor to be embedded into mechanical structures for in-situ temperature monitoring at highly elevated temperatures. Additive Manufacturing (also called 3D printing) using Selective Laser Melting (SLM) or Layered Metal Deposition (LMD) are two routes towards embedding such sensors into metallic structures to permit temperature sensing from within a metallic component. Work on this is in progress and is reported elsewhere [27].

Acknowledgment

This project has received funding from the European Union's Seventh Framework Programme for research, technological development and demonstration under grant agreement no 310279.

REFERENCES

[1] S. Pal, J. Mandal, T. Sun, K. T. V. Grattan, M. Fokine, F. Carlsson, P. Y. Fonjallaz, S. A. Wade and S. F. Collins, "Characteristics of potential fibre Bragg grating sensor-based devices at elevated temperatures," *Meas. Sci. Technol.*, vol. 14, no. 7, pp. 1131, Jun 2003.

[2] J. Canning, S. Bandyopadhyay, M. Stevenson, P. Biswas, J. Fenton, M. Aslund, "Regenerated gratings," *J. Eur. Opt. Soc. Rapid Pub.*, vol. 4, no. 09052, Dec. 2009.

[3] E. Lindner, C. Chojetzki, S. Brückner, M. Becker, M. Rothhardt, and H. Bartelt. "Thermal regeneration of fiber Bragg gratings in photosensitive fibers," *Opt. express*, vol. 17, no. 15, pp. 12523-12531, Jul 2009.

[4] S. J. Mihailov, "Fiber Bragg grating sensors for harsh environments," *Sensors*, vol. 12, no. 2, pp. 1898-1918, Feb. 2012.

[5] M. Fokine, "Thermal stability of oxygen-modulated chemical-composition gratings in standard telecommunication fiber," *Opt. lett.*, vol. 29, no. 11, pp. 1185-1187, June 2004.

[6] T. L. Lowder, K. H. Smith, B. L. Ipson, A. R. Hawkins, R. H. Selfridge, and S. M. Schultz, "High-temperature sensing using surface relief fiber Bragg gratings," *IEEE Photon. Technol. Lett.*, vol. 17, no. 9, pp. 1926-1928, Sept. 2005.

[7] C. E. Lee, R. A. Atkins, and H. F. Taylor, "Performance of a fiber-optic temperature sensor from -200 to 1050°C," *Opt. Lett.*, vol. 13, no. 11, pp. 1038-1040, Nov. 1988.

[8] T. Zhu, T. Ke, Y. Rao, and K. S. Chiang, "Fabry-Perot optical fiber tip sensor for high temperature measurement," *Opt. Commun.*, vol. 283, no. 19, pp. 3683-3685, Oct. 2010.

[9] O. Schneller, J. Mathew, W. N. MacPherson, and R. R. J. Maier, "High temperature sensor based on an in-fibre Fabry-Perot cavity," *Proc. SPIE*, vol. 9157, pp. 91578L, June 2014.

[10] G. W. Tregay, P. R. Calabrese, P. L. Kaplin, and M. J. Finney, "Optical fiber sensor for temperature measurement from 600 to 1900C in gas turbine engines," *Proc. SPIE*, vol. 1589, pp. 38-47, Dec. 1991.

[11] G. W. Tregay, P. R. Calabrese, M. J. Finney, and K. B. Stukey, "Durable fiber optic sensor for gas temperature measurement in the hot section of turbine engines," *Proc. SPIE*, vol. 2295, pp. 156-163, Oct. 1994.

[12] T. Habisreuther, T. Elsman, Z. Pan, A. Graf, P. Ahonen, K. Grujic, S. Simonsen, H. Mathisen, R. Norheim, R. Willsch, and M. Schmidt, "Long-term stable sapphire Fiber Bragg Grating sensors at 1400 C," *Proc. SPIE*, vol. 9157, pp. 915719-1, June 2014.

[13] T. Elsmann, T. Habisreuther, M. Rothhardt, R. Willsch, and H. Bartelt, "Advanced fabrication and calibration of high-temperature sensor elements based on sapphire fiber Bragg gratings," *Proc. SPIE*, vol. 9157, pp. 91572N, June 2014.

[14] A. Wang, S. Gollapudi, R. G. May, K. A. Murphy, and R. O. Claus, "Advances in sapphire-fiber-based intrinsic interferometric sensors," *Opt. lett.*, vol. 17, no. 21, pp. 1544-1546, Nov.1992.

[15] Y. Zhu, Z. Huang, F. Shen, and A. Wang, "Sapphire-fiber-based white-light interferometric sensor for high-temperature measurements," *Opt. lett.*, vol. 30, no. 7, pp. 711-713, Apr. 2005.

[16] J. Wang, B. Dong, E. Lally, J. Gong, M. Han, and A. Wang, "Multiplexed high temperature sensing with sapphire fiber air gap-based extrinsic Fabry–Perot interferometers," *Opt. lett.*, vol. 35, no. 5, pp. 619-621, Mar. 2010.

[17] D. A. Jackson, and J. D. C.Jones, "Extrinsic fibre-optic sensors for remote measurement: Part one," *Opt. Laser Technol.*, vol. 8, no. 5, pp. 243-252, Oct. 1986.

[18] A. Othonos, "Fiber Bragg gratings," *Rev. Sci. Instrum.*, vol. 68, no. 12, pp. 4309-4341, Dec. 1997.

[19] C. Ma and A. Wang, "Signal processing of white-light interferometric low-finesse fiber-optic Fabry–Perot sensors," *Appl. Opt.*, vol. 52, no. 2, pp. 127-138, Jan. 2013.

[20] M. Han, "Theoretical and experimental study of low-finesse extrinsic Fabry-Perót interferometric fiber optic sensors," PhD dissertation, Bradley Dept. Elect. Eng., Virginia Tech, Blacksburg, Virginia, 2006.

[21] A. Ezbiri, and R. P. Tatam, "Interrogation of low finesse optical fibre Fabry-Pérot interferometers using a four wavelength technique," *Meas. Sci. Technol.*, vol. 7, no. 2, pp.117-120, 1996.

[22] J. M. Kilpatrick, W. N. MacPherson, J. S. Barton, and J. D. C. Jones, "Phase-demodulation error of a fiber-optic Fabry-Perot sensor with complex reflection coefficients," *Appl. Opt.*, vol. 39, no. 9, pp.1382-1388, Mar. 2000.

[23] G. Ghosh, "Temperature dispersion of refractive-indexes in some silicate fiber glasses," *IEEE Photon. Technol. Lett.*, vol. 6, no. 3, pp. 431-433, Mar. 1994.

[24] G. M. H. Flockhart, R. R. J. Maier, J. S. Barton, W. N. MacPherson, J. D. C. Jones, K. E. Chisholm, L. Zhang, I. Bennion, I. Read, and P. D. Foote, "Quadratic behaviour of fibre Bragg grating temperature coefficients," *Appl. Opt.*, vol. 43, no. 13, pp. 2744-2751, May 2004.

[25] Nuffield Foundation, "A giant silver mirror," http://www.nuffieldfoundation.org/practical-chemistry/giant-silver-mirror, [Accessed: November, 2014].

[26] D. Havermann, J. Mathew, W. N. MacPherson, R. R. J. Maier, and D. P. Hand, "In-situ Measurements with Fibre Bragg Gratings embedded in Stainless Steel," *Proc. SPIE*, vol. 9157, pp. 9157A1, Jun. 2014.

[27] D. Havermann, J. Mathew, W. N. MacPherson, R. R. J. Maier, and D. P. Hand,, "Temperature and Strain Measurements with Fibre Bragg Gratings Embedded in Stainless Steel 316," *J. lightwave technol.*, accepted for publication.